Composites: Part A 61 (2014) 216–223

Contents lists available at ScienceDirect

Composites: Part A

journal homepage: www.elsevier.com/locate/compositesa

Embedded ferromagnetic microwires for monitoring tensile stress in polymeric materials

Dmitriy Makhnovskiy [a,*], Vlad Zamorovskii [b], John Summerscales [b]

[a] School of Computing and Mathematics, Plymouth University, Plymouth, Devon PL4 8AA, United Kingdom
[b] School of Marine Science and Engineering, Plymouth University, Plymouth, Devon PL4 8AA, United Kingdom

ARTICLE INFO

Article history:
Received 29 November 2013
Received in revised form 17 February 2014
Accepted 4 March 2014
Available online 12 March 2014

Keywords:
A. Smart materials
B. Stress transfer
C. Analytical modelling
D. Non-destructive testing

ABSTRACT

Considerable efforts have been made to develop testing non-destructive methods for polymer composite materials. We would like to introduce researchers in the field of smart materials to a new method of monitoring internal stresses. The method can be classified as an embedded sensing technique, where the sensing element is a glass-coated ferromagnetic microwire with a specific magnetic anisotropy. With a diameter 10–100 μm, the microwire impedance acts as the controlled parameter which is monitored for a weak alternating current (AC) in the MHz range. The microwire impedance becomes stress sensitive in the presence of a weak constant axial bias magnetic field. This external parameter allows the impedance stress sensitivity to be easily tuned. In addition, a local bias field may also allow the reconstruction of stress profile when it is scanned along the microwire. The experimental results are analysed using simple magnetostatic and impedance models.

1. Introduction

Ferromagnetic microwires coated with glass can be used in several niche applications due to their specific magneto-anisotropic properties [1–3]. There are two types of microwires. The first type, known as bistable microwires, is characterised by an almost rectangular magnetic hysteresis loop measured along the microwire axis. These microwires, demonstrating natural ferromagnetic resonance, have found applications in microwave absorbing materials [4–6]. The second type of microwires is characterised by a narrow inclined hysteresis loop. The most remarkable property observed in these microwires is the so-called magneto-impedance (MI) effect: a large change in the microwire high frequency impedance under the influence of a longitudinal magnetic field [7,8]. The Mohri et al. review [9] describes implemented magnetic sensors based on MI.

In the embedded sensing techniques, some special particles or fibres are used which act as mediators between internal parameters of the medium and a readout device. Depending on the physical principle of this intermediary function, different physical quantities can be utilised as the measurement parameters which include: current, voltage, resistance or impedance, electric or magnetic fields, permeability or permittivity, reflected or transmitted electromagnetic waves (amplitude and phase). The method of monitoring the internal tensile stresses, developed in the present work, consists in embedding a MI glass-coated microwire into a polymer matrix and measuring its impedance using a weak high frequency current in the MHz range. As opposed to the usual MI, the tensile stress is used as the control parameter instead of the magnetic field. Before we proceed, it would be useful to conduct a comparative analysis of several embedded sensing methods which are similar to our method either by the geometry of inclusions or some physical principles.

The undisputed leader in non-destructive testing of composites is the method using embedded optical fibres [10,11]. The silica or polymer optical fibre may play the role of a sensor by itself or could transmit signals between the tested area, where the light interacts with a substance, and a readout device. Along with the extraordinary sensitivity, the optical method can also measure a wide range of parameters such as strain, temperature, pressure, humidity, and vibration. In addition, it is immune to electromagnetic interference. The experience gained by the integration of optical fibres into a polymer matrix is useful to us because their diameters (7–50 μm) are close to those of microwires. Since microwires are coated with glass, the bonding of matrix–microwire and matrix–fibre interfaces should be comparable assuming similar surface treatments. Despite modest diagnostic capabilities as compared with optical

* Corresponding author.
E-mail addresses: D.Makhnovskiy@plymouth.ac.uk (D. Makhnovskiy), Vlad.Zamorovskii@plymouth.ac.uk (V. Zamorovskii), J.Summerscales@plymouth.ac.uk (J. Summerscales).

http://dx.doi.org/10.1016/j.compositesa.2014.03.006
1359-835X/

fibres, the microwire-based sensor proposed in our work can be made tuneable and the instrumentation has much lower cost.

In impedance-based spectroscopy [12–16], the effective impedance of the mixture of conductive reinforcing fibres (steel or carbon) and a weakly conductive matrix is measured in a specific frequency range (normally MHz) between a pair of patch contacts attached to the sample surface. Since the volume fraction of fibres (<3%) is usually below the percolation transition, the presence of a weakly conductive matrix is absolutely necessary to ensure the effective conductivity. An external stress does not change the electrical properties of non-magnetic conductive fibres. The piezoimpedance effect is caused by the fibre–matrix interface which has a capacitive nature due to the oxidation or polarization layers forming on the surfaces of steel and carbon fibres, respectively. Thereby, this method can scarcely be used in polymer matrixes as the conductivity is too small. On the contrary, the stress sensitivity of ferromagnetic microwires is caused only by their internal magnetic properties, and hence they can be used in any dielectric matrix allowing their embedding.

In magnetostrictive tagging, Terfenol-D magnetic microparticles (<300 μm in size) are added to the composite matrix to produce the effective magnetic properties [17,18]. Since Terfenol-D particles are almost nine times denser than the matrix resin, they tend to settle during cure. To prevent this process, the sample is placed between the poles of a permanent magnet creating a homogeneous magnetic field perpendicular to the sample plane. Samples manufactured using this technique have aligned particle clusters and demonstrate an enhanced magnetostrictive response when they are loaded. Stress transferred through the matrix to the particles causes a change in the direction of equilibrium magnetisation due to the inverse magnetostrictive effect. Stress monitoring measures the longitudinal or transverse component of the magnetic field near the sample surface using a magnetometer. This inverse magnetostriction effect is also used in our method. However the measured quantity is a high frequency MI of microwires that depends on the direction of magnetisation. The use of ready-made microwires eliminates the necessity of forming the magnetic properties during cure. Moreover, the MI microwires have a very narrow hysteresis loop that eliminates the problem of calibration when measuring a cyclic load.

Investigation of the matrix parameters which may affect the magneto-impedance of embedded microwires is of crucial importance for the development of not only the contact stress sensors, but also microwave smart materials. In the GHz range, microwires homogeneously distributed inside the matrix can be interrogated remotely using microwave beams. The short microwire inclusions will scatter the incident microwave in a similar manner to the miniature dipoles [19], while the long microwire strings will respond as the cold plasma of free electrons [20]. A local magnetic field, stress, and temperature will change the impedance of microwires and, as a consequence, the transmitted and reflected microwaves. The volume fraction of microwires required to introduce a tuneable microwave functionality is very small (much less than 1%) and thus reduces the impact of sensor inclusions on the mechanical properties of matrix. Composites based on ferromagnetic micro- and nano-microwires are being studied experimentally and theoretically by several research groups (see e.g. [21–26]). Despite the growing interest in tuneable microwave composites, to our knowledge only one work [27] has been published where the effect of tensile stress on the free-space microwave properties of the wire-filled composites was demonstrated. Difficulty in carrying out such experiments is caused by the need to integrate a loading frame with microwave antenna measurements.

In our present work, we return to contact impedance measurements with a ferromagnetic microwire embedded into a commercial epoxy resin matrix. Our experiments are designed not only to demonstrate the physical effects, but also to address a number of practical issues that pertain to the embedded sensors. In particular, we show how the magnetic and mechanical response of microwires are related to the matrix elastic properties.

2. Magnetostatic and impedance models for glass-coated microwires

In this section we introduce the magnetostatic and impedance models used in Section 3 to analyse experimental results. The Gaussian-cgs system of units will be used within the formulation of theoretical models, while SI units are more convenient for the interpretation of experimental data. Unless it is otherwise, the physical dimensions specified in the brackets would refer to SI units.

2.1. Magnetostatic model for glass-coated microwires

Glass-coated microwires are produced using the Taylor–Ulitovskiy casting method [1,2]. As a result of quenching, an amorphous or polycrystalline metal core is obtained in the glass envelope. The initial process of quenching and the difference in thermal expansion coefficients of glass and metal create a tensorial residual stress, $\hat{\boldsymbol{\sigma}}$, inside the metal core which is responsible for the magnetic anisotropy [28–30]. The components of $\hat{\boldsymbol{\sigma}}$ can be further modified by an annealing treatment. In as-cast glass-coated microwires, the axial tensile stress σ_a produced by the glass shell is predominant over other residual stresses. For glass-coated microwires made of a Co-based alloy, which have a small negative magnetostriction, the predominant residual tensile stress σ_a will result in a circular magnetisation $\mathbf{M}_0$ in the near-surface layer of the metal core. In turn, this circular magnetised shell is divided into cylindrical domains with opposite magnetisation directions.

The direction of $\mathbf{M}_0$ can be controlled by the combined action of an external axial magnetic field H_{ex} and an external axial stress σ_{ex}. The total residual stress on the surface of the microwire metal core also needs to be taken into account. It can be decomposed into the axial tension σ_1 ($\sigma_1 = \sigma_a$) and the torsion (pure shear) which is a combination of tension and compression with equal intensity σ_2 perpendicular to each other and at 45° to the microwire axis [31]. In the frame of the Stoner–Wohlfarth model [32], the total magnetostatic energy per unit volume (erg/cm^3, cgs) can be written in the following form [33]:

$$U_t(\theta) = -M_0\left(\frac{1}{2}\mathrm{sgn}(\lambda)H_K\cos^2(\alpha+\theta) + H_{ex}\cos(\theta) + H_b\sin(\theta)\right) \quad (1)$$

$$K = \frac{3}{2}|\lambda|\tilde{\sigma} \quad (2)$$

$$H_K = \frac{2K}{M_0} = \frac{3|\lambda|\tilde{\sigma}}{M_0} \quad (3)$$

$$\alpha = \frac{1}{2}\tan^{-1}\left(\frac{2\sigma_2}{\sigma_1+\sigma_{ex}}\right) \quad (4)$$

$$\tilde{\sigma} = \sqrt{(\sigma_1+\sigma_{ex})^2 + 4\sigma_2^2} \quad (5)$$

where α is the angle of magnetic anisotropy measured from the circular direction, $\mathrm{sgn}(\lambda)$ is the sign of the magnetostriction constant λ, K is the anisotropy constant (erg/cm^3, cgs), H_K is the anisotropy field (Oe, cgs), $H_b = 2I_b/ca$ (Oe, cgs) is the circular DC magnetic field on the surface of metal core induced by a DC bias current I_b in the microwire, θ is the angle between $\mathbf{M}_0$ (emu/cm^3, cgs) and the wire axis, $M_0 = |\mathbf{M}_0|$ is the module of $\mathbf{M}_0$, the parameters $\sigma_{1,2}$ (dyn/cm^2,

cgs) are assumed to be positive, the external axial stress σ_{ex} (dyn/cm^2, cgs) may be positive (tension) or negative (compression), The current I_b may improve the experimental MI characteristics by eliminating the circular domain structure [34].

The equilibrium direction of $\mathbf{M}_0(\theta_{eq})$ is found by minimizing the magnetostatic energy: $\partial U_t(\theta)/\partial\theta = 0 \rightarrow \theta = \theta_{eq}$. For $\lambda < 0$, in accordance with the principle of minimum energy, the axial tension will rotate $\mathbf{M}_0$ towards the circular direction ($\theta \rightarrow 90°$), while the crossed tension and compression will rotate $\mathbf{M}_0$ towards a 45° axis. Thus, there are two competing rotations. As a result, in the absence of H_{ex} the equilibrium angle will be $45° \leqslant |\theta| \leqslant 90°$ with respect to the 0° axial microwire direction.

2.2. Impedance model for ferromagnetic microwires

The voltage V (V) measured across a microwire with a length l (m) carrying an alternating current $i = i_0\exp(-j\omega t)$ (A) can be expressed through the ζ_{zz} component of the impedance tensor $\hat{\zeta}$ (Ω) relating the axial electric field e_z (V/m) and the circular magnetic field h_φ (A/m) induced by the current [34]:

$$V = e_z l = \zeta_{zz} h_\varphi l \tag{6}$$

Here, $h_\varphi = i/2\pi a$ (SI) is the circular magnetic field on the surface of the microwire metal core having a radius a (m). Eq. (6) can be rewritten in the form of Ohm's law: $V = iZ$, where $Z = \zeta_{zz} l/2\pi a$ (Ω) is the microwire impedance (complex resistance). The surface impedances in the two systems of units can be easily recalculated into each other: $\zeta^{cgs} = (10^9/4\pi c) \times \zeta^{SI} \approx 0.002654 \times \zeta^{SI}$ (dimensionless in cgs), where ζ is a component of $\hat{\zeta}$ and $c \approx 3.0 \times 10^{10}$ cm/s is the speed of light. The surface longitudinal impedance ζ_{zz} can be recovered from the measured microwire impedance Z: $\zeta_{zz}^{SI} = 2\pi a Z/l$ or $\zeta_{zz}^{cgs} = 10^9 aZ/(2cl)$. During the measurements, the interpretation of Z or ζ_{zz} as a lumped parameter is true only if the length l of microwire sample is much smaller than the effective wavelength.

In Ref. [34], the component ζ_{zz} was calculated at the conditions of weak and strong current skin-effects:

$$\zeta_{zz}^{weak}(\theta) \approx \frac{kc\rho}{4\pi}\frac{J_0(ka)}{J_1(ka)} \tag{7}$$

$$\zeta_{zz}^{strong}(\theta) \approx \frac{(1-j)}{2}\sqrt{\frac{\omega\rho}{2\pi}}\left(\sqrt{\mu_{eff}(\theta,\omega)}\cos^2(\theta) + \sin^2(\theta)\right) \tag{8}$$

where $J_{0,1}$ are the Bessel functions of the first kind, ρ is the specific resistivity (s, cgs), a is the microwire radius (cm, cgs), $\mu_{eff} = 1 + 4\pi\chi$ is the effective permeability, $\gamma \approx 1.8 \times 10^7$ (rad $\times$ s^{-1} $\times$ Oe^{-1}, cgs) is the gyromagnetic ratio, and $\tau \ll 1$ is a small spin-relaxation parameter. Other dynamic parameters are:

$$k^2 = \frac{4\pi j\omega(1 + 4\pi\cos^2(\theta)\chi)}{\rho c^2},$$

$$\chi = \frac{\omega_M(\omega_2 - j\tau\omega) + 4\pi\omega_M^2}{(\omega_1 - j\tau\omega)(\omega_2 + 4\pi\omega_M - j\tau\omega) - \omega^2},$$

$$\omega_1 = \gamma(H_{ex}\cos\theta + H_b\sin\theta - H_K\cos 2(\alpha+\theta)),$$

$$\omega_2 = \gamma(H_{ex}\cos\theta + H_b\sin\theta + H_K\sin^2(\alpha+\theta)),$$

$$\omega_M = \gamma M_0.$$

Note that in Ref. [34] α was measured from the microwire axis, while in the above equations it is measured from the radial direction. A criterion should be proposed to choose between Eqs. (7) and (8) as these asymptotic formulae do not transform into each other when changing the frequency. The high frequency approximation (8) has to be used when $\delta_m/a \ll 1$, where $\delta_m = c\sqrt{\rho/(2\pi\omega|\mu_{eff}|)}$ is the so-called magnetic skin-depth.

3. Microwire stress-impedance and its application to the tensile stress monitoring of polymer composite materials

It will be shown that a longitudinal DC bias field is required to provide the tensile stress sensitivity of microwire impedance. The stress transformation properties of magneto-impedance characteristics measured in a microstrip cell in the MHz range are in a good agreement with the model formulated in Section 2. However, the stress impedance measurements conducted for a microwire embedded into a composite matrix reveal a significant discrepancy with the model and the stress impedance measurements in the RF cell. Some possible reasons of the discrepancy are discussed in this section.

3.1. Stress-impedance in the presence of a longitudinal DC bias field

Diameters of typical glass-coated microwires are in the range of 5–50 μm, and hence they can be easily embedded between individual layers of a composite structure. For the stress-monitoring, we used Co-based microwires with the composition $Co_{68}Fe_4Cr_3Si_{11}B_{14}$ (wt%) provided by MFTI Ltd (Republic of Moldova). The diameter of metal core and the thickness of glass shell were ~25.3 μm and ~4 μm, respectively. The magnetisation curves $M_{axial}(H_{ex}) = M_0\cos(\theta(H_{ex}))$ shown in Fig. 1 were measured for a 5 cm long microwire by means of the inductive method. The loops observed at the saturation region were caused by non-ideal balancing of the electronic circuit. In the middle part of magnetisation curves, magnetic hysteresis may also contribute to the loop opening. During these measurements, the upper end of the microwire was fastened, while its lower free end was loaded with different weights of mass M (grams) to produce an external tensile force $F = Mg$, where $g \approx 9.8$ m/s^2 is the gravitational acceleration. This stress is redistributed between the metal core of the microwire and its glass shell which each have different Young's moduli (E_m, E_g) and cross-sections (S_m, S_g), where subscripts m and g indicate metal core and glass shell respectively. The stress σ_{ex} in Eqs. (3)–(5) transferred to the metal core can be calculated on the basis of the principle of consistent deformations used in statically indeterminate systems:

$$\sigma_{ex} = \frac{E_m F}{E_m S_m + E_g S_g} \tag{9}$$

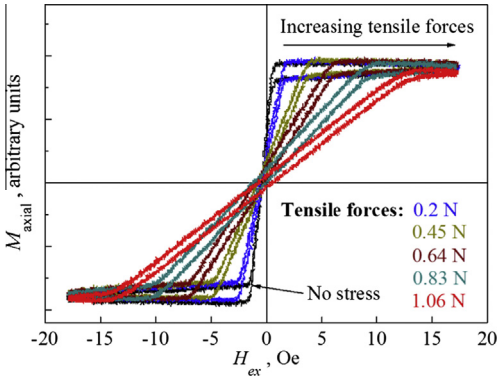

Fig. 1. The experimental magnetisation curves measured in the $Co_{68}Fe_4Cr_3Si_{11}B_{14}$ microwire at different tensile forces. The microwire has the total diameter ~33.3 μm, the metal core diameter ~25.3 μm, and the thickness of glass shell ~4 μm. (For interpretation of the references to colour in this figure legend, the reader is referred to the web version of this article.)

To estimate this stress in a glass-coated amorphous CoFeSiB microwire, the typical Young's moduli would be $E_m \sim 130$ GPa and $E_g \sim 70$ GPa [35].

The presence of linear central parts in the narrow hysteresis loops shown in Fig. 1 is a characteristic feature of glass-coated ferromagnetic microwires with a circular magnetic anisotropy ($\alpha \approx 0$). For these microwires, the transition from the inclined central part to the saturation region occurs at $H_{ex} = \pm H_K$. The anisotropy angle $\alpha \approx 0$ in Eq. (4) is measured from the circular direction and is achieved for $\sigma_1 \gg \sigma_2$ when the axial residual stress prevails over other residual stresses. Using Eqs. (3) and (5) with $\sigma_1 \gg \sigma_2$ and Eq. (9), the residual tensile stress σ_1 can be estimated as:

$$\sigma_1 \sim \frac{\sigma_{ex} H_K(0)}{H_K(\sigma_{ex}) - H_K(0)} \tag{10}$$

where $H_K(0)$ and $H_K(\sigma_{ex})$ are the experimental anisotropy fields taken from Fig. 1 at $\sigma_{ex} = 0$ and any $\sigma_{ex} \neq 0$, respectively. For an experimental value $F = 1.06$ N (see Fig. 1), Eq. (9) gives $\sigma_{ex}(1.06N) \approx 1.512$ GPa. Putting $H_K(0) \approx 2$ Oe and $H_K(1.512\text{GPa}) \approx 13$ Oe (both taken from Fig. 1) into Eq. (10), we obtain $\sigma_1 \sim 275$ MPa. The failure force $F_f = 1.42$ N produces the tensile stress $\sigma_{ex} \sim 2$ GPa in the metal core.

The magnetostatic model in Eqs. (1)–(5) reproduces the experimental magnetisation curves and their transformations under the effect of external tensile stress. In Fig. 2, the theoretical curves $\cos(\theta(H_{ex})) = M_{\text{axial}}(H_{ex})/M_0$ were calculated for the following model parameters: $\sigma_1 = 275 \times 10^7$ dyn/cm^2 (from the estimated 275 MPa), $\sigma_2 = 5 \times 10^7$ dyn/cm^2 (any arbitrary value that provides a small loop opening), $\lambda = -10^{-7}$ (a typical value), $M_0 = 400$ emu/cm^3 (estimated from $M_0 = 3|\lambda|\sigma_1/H_K(0)$), and $H_b = 0$. The parameter σ_2 controls the width of hysteresis loop (very small in our microwire). On increasing the external stress, the anisotropy field $H_K(\sigma_{ex}) = 3|\lambda|\sqrt{(\sigma_1 + \sigma_{ex})^2 + 4\sigma_2^2}/M_0$ as a function of σ_{ex} also increases, while the anisotropy angle α from Eq. (4) measured from the circular direction becomes smaller.

Since $Z \sim \zeta_{zz}$, further analysis will be conducted for ζ_{zz}. In Fig. 3, the field dependencies of $|\zeta_{zz}|$ with the tensile stress σ_{ex} as the variable parameter were calculated for a microwire with an almost circumferential anisotropy ($\alpha \approx 0$) using Eqs. (1)–(5), (and) (8). The excitation frequency was chosen to be 40 MHz (one of experimental frequencies used in Section 3.2). The magnetostatic parameters used for the calculations were the same as in Fig. 2. Other parameters used: $a = 12.65 \times 10^{-4}$ cm is the radius of microwire metal core and $\rho = 2.56 \times 10^{-16}$ (s, cgs) is its resistivity (estimated from experimental data), $\gamma = 1.8 \times 10^7$ (rad $\times$ s^{-1} $\times$ Oe^{-1}, cgs) is the gyromagnetic ratio, and $\tau = 0.01$ is a small relaxation parameter. As seen in Fig. 3, under the effect of tensile stress, the curve $|\zeta_{zz}(H_{ex})|$ becomes wider. The maxima of $|\zeta_{zz}(H_{ex})|$ are reached at $H_{ex} = \pm H_K$ (see Eq. (3)). In zero magnetic field, ζ_{zz} does not show any stress sensitivity because the magnetisation angle is already 90°, and hence the direction of equilibrium magnetisation $\mathbf{M}_0$ will not be changed by an external tensile stress. For $H_{ex} \neq 0$, the magnetisation will be deflected from its initial circular direction. In this case, ζ_{zz} becomes stress sensitive because the external tensile stress will rotate the magnetisation back to the circular direction. The largest stress sensitivity of ζ_{zz} is achieved at $H_{ex} = \pm H_K(0)$, where $H_K(0)$ is H_K at $\sigma_{ex} = 0$. For these bias fields, the saturation stress σ_s required to rotate the magnetisation back to nearly 90° is of the order of σ_1 (residual axial tensile stress). Using Eq. (3), σ_1 can be expressed through the anisotropy field. For the saturation strain $\varepsilon_s = \sigma_s/E_m \sim \sigma_1/E_m$, we obtain ($\sigma_1 \gg \sigma_2$):

$$\varepsilon_s \sim \frac{H_K(0) M_0}{3|\lambda| E_m} \tag{11}$$

where E_m (dyn/cm^2, cgs) is the Young modulus of the metal core. The anisotropy fields of glass-coated microwires are typically in the range 1–20 Oe.

The experimental field dependencies of $|Z(H_{ex})| \sim |\zeta_{zz}(H_{ex})|$ shown in Fig. 4 were measured for the same $Co_{68}Fe_4Cr_3Si_{11}B_{14}$ microwire as in Fig. 1. The measurement method is described below. A short piece of the microwire (~20 mm) is placed onto a PCB microstrip measurement cell (MMC) as shown in Fig. 4. To

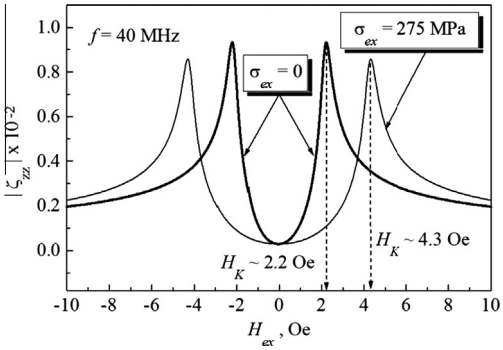

Fig. 3. The theoretical field dependencies of ζ_{zz} with σ_{ex} as a parameter calculated for a microwire with an almost circumferential anisotropy using Eq. (8) and the magnetostatic model (1)–(5). The excitation frequency is 40 MHz.

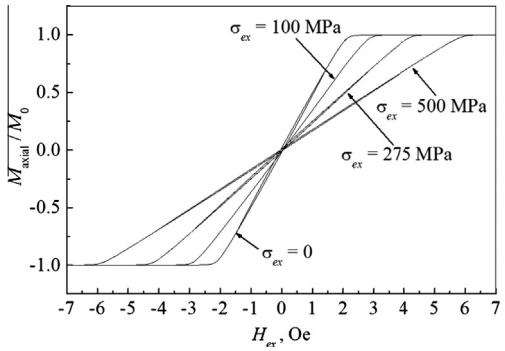

Fig. 2. The theoretical magnetisation curves with the external tensile stress as a parameter calculated for a microwire with an almost circumferential anisotropy using the magnetostatic model (1)–(5). The model parameters used for the calculations are: $\sigma_1 = 275 \times 10^7$ dyn/cm^2, $\sigma_2 = 5 \times 10^7$ dyn/cm^2, $\lambda = -10^{-7}$, and $M_0 = 400$ emu/cm^3. A small σ_2 was used to reproduce the narrow hysteresis loops observed in the experiment.

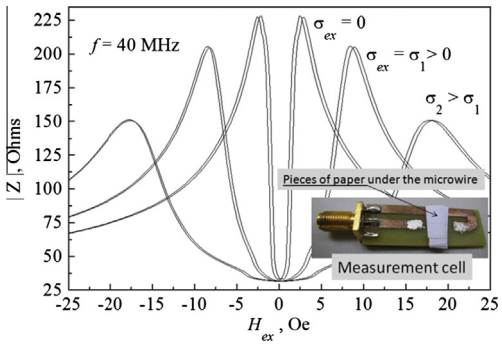

Fig. 4. The microwire impedance vs. the axial magnetic field measured in the same $Co_{68}Fe_4Cr_3Si_{11}B_{14}$ microwire as in Fig. 1 at different tensile stresses. The microstrip measurement cell is also shown. The excitation frequency was 40 MHz. The tensile stress was introduced by means of the pieces of paper placed under the microwire to slightly stretch it. (For interpretation of the references to colour in this figure legend, the reader is referred to the web version of this article.)

enable the electrical contacts, the glass coating at the ends of microwire is mechanically removed and then the microwire ends are attached to the microstrips using a conductive glue or paint. The MMC has a single 3.5 mm connector between the ground plane and the microstrip. The 1-Port standard load calibration procedure is performed to calibrate the coaxial measurement track between the cell (before the 3.5 mm connector) and the Analyser's port. In a lower band of the MHz range, the microstrips will not introduce significant distortions in the microwire impedance response. The microwire impedance is calculated from the measured S_{11} parameter (a complex reflection coefficient) as $Z = 50\Omega \times (1 + S_{11})/(1 - S_{11})$. The microwire was fixed within the MMC strip gap using a conductive paint at positions 15 mm apart. Tensile stress was introduced by inserting up to 5 pieces of paper under the central 5 mm of the microwire to raise the middle of the microwire by ~0.1 mm per piece of paper. The geometrical parameters of each piece of paper (width ~5 mm and thickness ~0.1 mm) and the strip gap (15 mm) permit estimation of the maximum strain for 5 pieces as 3.33×10^{-3} as shown in Fig. 4. Whilst using such a method, the stress cannot be accurately controlled, but its effect on $|Z(H_{ex})|$ can be clearly demonstrated. The experimental field dependencies of $|Z(H_{ex})|$ shown in Fig. 4 and their stress-transformational properties are in qualitative agreement with the theoretical ones in Fig. 3.

Figs. 3 and 4 demonstrate that the magnetostatic and impedance models (1)–(8) will work well at least for the chosen microwire. However, these models remain oversimplified. The kHz range and the lower band of MHz range are always problematic for the impedance model (7), (8) as they completely neglect the domain structure and the corresponding susceptibility caused by the high frequency oscillations of domain walls. Fig. 5 shows the typical behaviour of the field impedance measured in a Co-based microwire at a low MHz frequency. Now, the minimum impedance in zero field is not global. Furthermore, as the frequency goes down, this minimum impedance moves up and finally transforms into the global maximum. All these effects are due to the domain susceptibility which is not included into our model. A moderate tensile stress will make the minimum at zero field deeper. The anisotropy field increases with the application of tensile stress. Thus, at lower MHz frequencies, a microwire becomes stress-sensitive even in zero field. However, such stress sensitivity is of little interest for monitoring purposes due to its irregularity. Actually, the field characteristic of $|Z(H_{ex})|$ at 1 MHz can be made similar to that of 40 MHz by applying a small DC bias current (tens mA) through the microwire. Such current will eliminate the circular domain structure thereby making the impedance model more suitable [34]. The model will work better for higher band MHz range and GHz frequencies where the oscillations of domain walls are strongly damped.

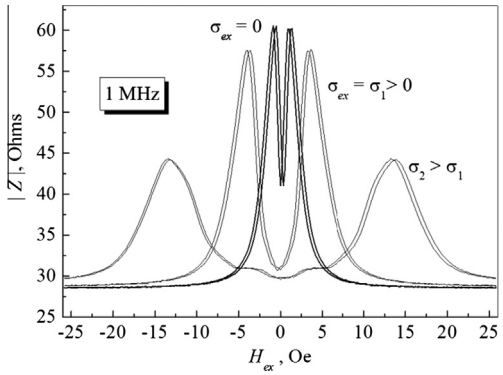

Fig. 5. The typical behaviour of the field impedance at lower MHz frequencies. The impedance was measured in the same microstrip cell as in Fig. 4.

3.2. Monitoring of internal tensile stress in polymer materials using the microwire stress-impedance

The experimental setup used for the stress impedance measurements is shown in Fig. 6. It comprises an Agilent 8753E Vector Network Analyser, a 3.5 mm coaxial cable between the microwire and the Analyser, a bias magnetic coil (short solenoid) wound around the test part of the sample, and a Instron 5582 screw-driven universal test machine. The complex-valued microwire impedance is calculated as $Z = 50\Omega \times (1 + S_{11})/(1 - S_{11})$. The dog-bone sample was made of a commercial epoxy resin without reinforcements (Sicomin SR8100 epoxy with SD8824 polyamine blend standard hardener resin system). Its test gauge length and cross-section are 70 mm and $5 \times 12\ mm^2$, respectively. A $Co_{68}Fe_4Cr_3Si_{11}B_{14}$ microwire was embedded into the epoxy resin during the sample fabrication along its length as shown in Fig. 7. Obtaining reliable electrical connections between external conductors and the glass-coated microwires remains one of the most serious problems for this type of sensor. The glass can be removed mechanically or chemically, and then the exposed end must be connected to a conductor while minimising mechanical stresses on the microwire. In our method, the ends of the microwire and an external wire connector are put into a miniature metal tube (clamp) from opposite sides and then strongly compressed. The compression destroys the glass coating on the microwire end and provides a reliable electrical contact with the external connector. To improve the contacts,

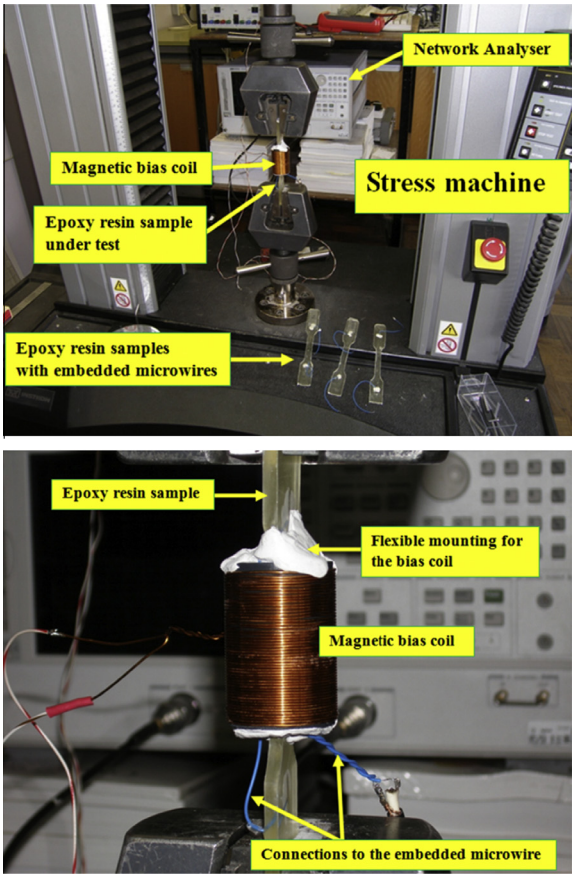

Fig. 6. The experimental setup and the test samples used for the stress impedance measurements. (For interpretation of the references to colour in this figure legend, the reader is referred to the web version of this article.)

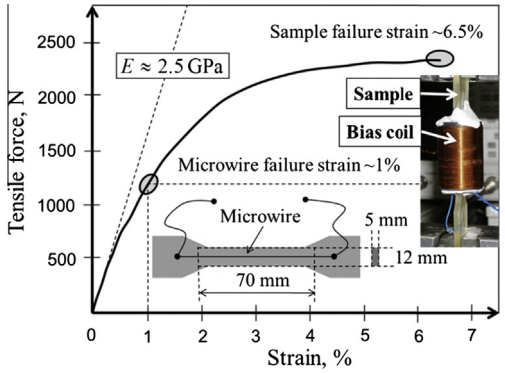

Fig. 7. The force-strain characteristic of the epoxy sample and its physical dimensions. Young's modulus E of the sample measured at the origin was ~2.5 GPa. The sample failure stress was ~38 MPa. (For interpretation of the references to colour in this figure legend, the reader is referred to the web version of this article.)

a conductive glue can be injected into the clamps before their compression. Both the contacts were then embedded into the matrix together with the microwire.

The force-strain characteristic of the sample in Fig. 7 is typical of viscoelastic materials where the elastic stress monotonically transforms into the plastic one without a yield plateau. Since the stress characteristics of viscoelastic materials are time-dependent even for a constant stress or a constant strain [35], the test conditions must be clearly specified. In Fig. 7, the stress was applied in the load steps with ~1 min time intervals. During the pauses, the microwire impedance was automatically measured at 11 frequency points within a fixed frequency range 1–40 MHz. This range was selected based on the dispersion properties of the stress impedance and some limitations associated with contact measurements. Below 1 MHz the stress impedance characteristics become irregular. For frequencies higher than 40 MHz, the electronic circuitry will be much more complicated, and also the microwire impedance response becomes very sensitive to the environment. The microwire failure strain ~1% was found by measuring the microwire DC resistance until it became infinite when the microwire broke. Young's modulus E measured at low strain was ~2.5 GPa. The sample failure strain and stress were ~6.5% and ~38 MPa, respectively.

The plots of the microwire impedance Z versus applied tensile force F are shown in Fig. 8 for three current excitation frequencies 1, 5 and 40 MHz, and at the different axial bias magnetic fields H_{ex} induced by the short solenoid. If no bias field is applied, for 1 MHz the impedance demonstrates irregular stress sensitivity with relatively small deflections from the mean. The field of 1.1 Oe does not make any difference. The radical change in $Z(F)$ occurs at H_{ex} = 2.1 Oe. For this field, the maximum stress sensitivity is observed. We already know that 2.1 Oe is the microwire anisotropy field $H_K(0)$ (see Fig. 3). For fields higher than $H_K(0)$, the slope of $Z(F)$ will shift toward greater stresses. A similar behaviour of the stress impedance characteristics is observed for 5 and 40 MHz, but the curves are more regular. The regularity of stress impedance curves measured for 1 MHz can be improved by passing a small DC bias current (tens of mA) through the microwire to eliminate the circular domain structure in the metal core [34]. Our measurements suggest that the current excitation frequency should be between 1 and 40 MHz. Within this range, it is advisable to choose the minimum frequency that provides a good impedance characteristic with/without a DC bias current. Further increase of the excitation frequency would be problematic for a contact sensor because the buffer impedance of the external connectors will contribute

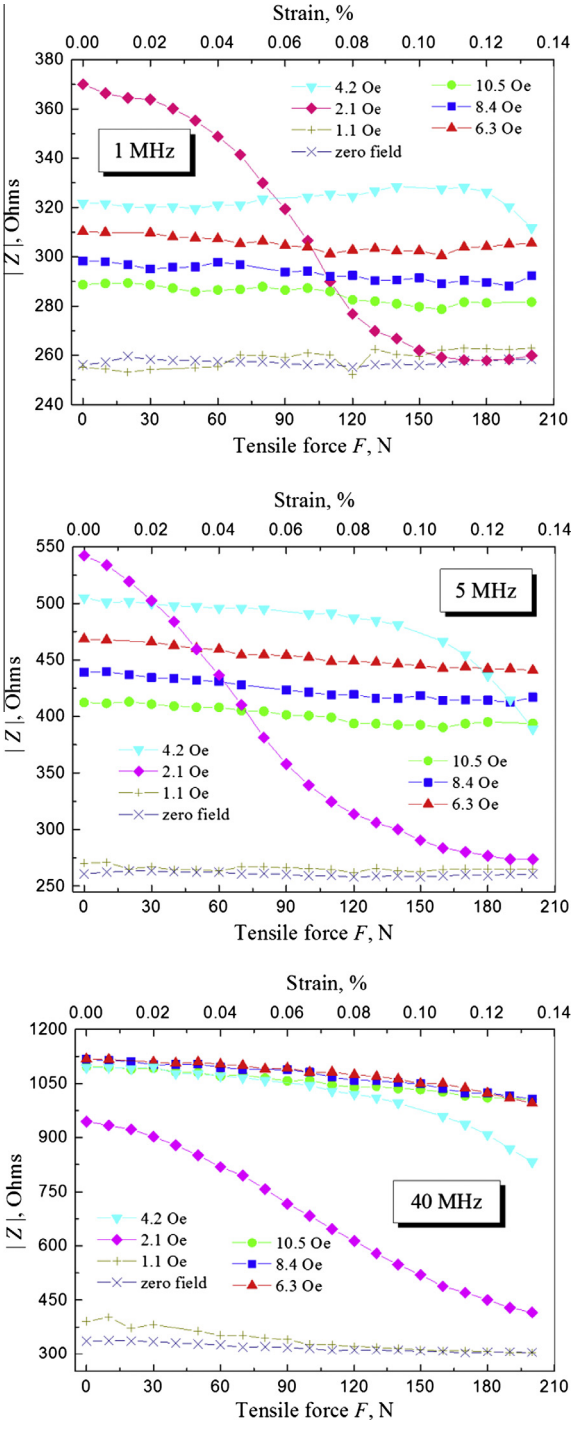

Fig. 8. The impedance vs. applied tensile stress measured at different axial bias fields for three excitation frequencies. (For interpretation of the references to colour in this figure legend, the reader is referred to the web version of this article.)

significantly to the total impedance, and thus reduce the stress sensitivity.

For the microwire used in our experiments, the strain ε_s saturating the impedance (see Eq. (11)) was about 0.08–0.14%. Such a small strain might be produced, for instance, by moderate heating of the sample without any external stress. Indeed, the coefficient of linear expansion of commercial epoxy resins lies in the range $(45–65) \times 10^{-6}$/°C [35], and hence an increase of temperature will result in $\geqslant$45 με/°C. Thus, a deliberate desensitisation of the stress impedance is absolutely essential for the practical use of this

method. According to Eq. (11), this can be done by increasing the anisotropy field. For the upper limit ~20 Oe, ε_s may be higher than 1 thus approaching the sample failure strain. Therefore, the microwire can be designed so that its magnetic properties will fit a certain range of external tensile stresses.

For stress monitoring applications, we need infallible bonding between the microwires and the matrix. To ensure this, the cure must be fully completed and the temperature gradually relaxed before the sample is exposed to environmental conditions. However, in service, temperature fluctuations may contribute to progressive debonding due to the difference in the thermal expansion of the microwire and the matrix. Also, we have the problem of the thermal stability of the magneto-impedance itself which will be affected by (i) the thermal drift of magnetic properties of the alloy and (ii) the change of magneto-elastic anisotropy due to the difference in thermal expansion coefficients of the metal core and the glass shell. The second effect may manifest itself at relatively low temperatures. Adenot-Engelvin et al. [36] have shown that nanocrystalline Finemet glass-coated microwires may demonstrate perfect thermal stability up to 300 °C. In principle, for certain microwires having a proper combination of the geometrical and structural properties, very stable impedance characteristics can be obtained. The development of such alloys and microwires should be continued with close collaboration between academic institutes and wire manufacturers.

For the excitation frequency 40 MHz, the model approach has been proven to qualitatively reproduce the experimental field impedance $|Z(H_{ex})|$ and its transformational properties under the effect of external tensile stress as shown in Figs. 3 and 4. This agreement remains at higher MHz frequencies. Therefore, at least for the frequencies higher than 40 MHz, the model should also reproduce the experimental stress impedance $|Z(F)|$ shown in Fig. 8. However, for a bias field larger than the anisotropy field ~2.1 Oe, the theoretical stress impedance $|\zeta_{zz}(\sigma_{ex})|$ will have a non-monotonic behaviour with the characteristic maximum similar to that shown in Fig. 9 for H_{ex} = 4 Oe. Such maxima are not observed in the experiment (see Fig. 8). In the theoretical dependence of the stress impedance, the maximum at a fixed bias field is unavoidable because it is reproduced from one of the impedance maxima in $|\zeta_{zz}(H_{ex})|$ (see Fig. 3) when it is shifted by the stress across the vertical line defined by a fixed field $|H_{ex}| > H_K(0)$. This is a purely geometrical effect. Certainly, the experimental field impedance $|Z(H_{ex})|$ in Fig. 4 and its transformations under the effect of tensile stress will reproduce exactly the same stress dependence of $|Z|$ at a fixed H_{ex}. To explain the absence of the maxima in Fig. 8, it should be recalled that $|Z(F)|$ was measured inside an epoxy matrix, while $|Z(H_{ex})|$ in Fig. 4 and its transformations by stress were measured for unembedded microwire on the top of a PCB microstrip cell. This discrepancy is probably caused by residual stresses

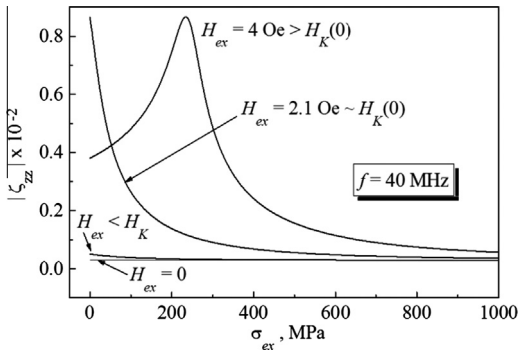

Fig. 9. The microwire impedance vs. applied tensile stress at different bias fields calculated using Eq. (8) and the magnetostatic model (1)–(5). The model parameters are the same as in Fig. 3. The excitation frequency is 40 MHz.

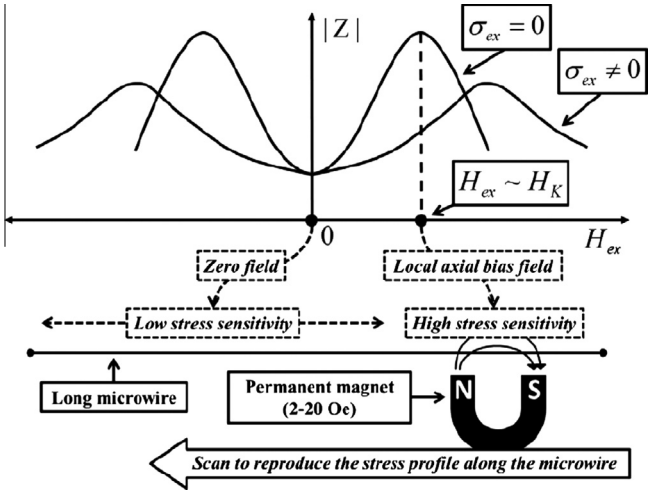

Fig. 10. The principle of local stress monitoring.

which are transferred to the microwire during embedding into the epoxy matrix and the ensuing curing processes. The stresses are cinput to the model through the magnetostatics (1)–(5) which has only four free parameters: a magnetisation M_0, a magnetostriction λ, a residual axial tensile stress σ_1, and a residual surface torsion stress σ_2. Varying both stresses, we have tried to reproduce the experimental curves in Fig. 8. The residual stresses in the microwire from embedding and cure cannot currently be completely described by our model. Nevertheless, for $|H_{ex}| < H_K(0)$, the model predicts a similar monotonous decrease of the stress impedance as in the experiment. A limitation of our approach might be the simplicity of our magnetostatic models. However, the real cause of the discrepancy with the experimental data in Fig. 8 for $|H_{ex}| > H_K(0)$ lies in the electrodynamic model (7), (8), where we completely neglect the radial distribution of magnetic properties inside the microwire. In the MHz range, the current skin-depth may not be sufficiently small for such assumption. In the GHz range, the model should work better because the excitation current will be strongly localised within a very thin layer near the surface, where the magnetic properties can be considered to be homogeneous. Furthermore, the functional behaviour of $|Z(H_{ex})|$ becomes much simpler at the GHz frequencies [37] as the module of impedance reaches its maximum values at $H_{ex} = \pm H_K(0)$ and then remains constant for any $|H_{ex}| > H_K(0)$. Consequently, the stress dependence of $|Z|$ at any fixed H_{ex} will be represented by a monotonically decreasing curve. Thus, the agreement between the theory and the experiment should be restored again.

In Fig. 8, the impedance characteristics measure a tensile stress averaged along the microwire because it was magnetically biased as a whole. Using such long sensing elements, local stress monitoring is also possible as explained in Fig. 10. A bias field induced by a weak permanent magnet can be applied locally to activate a small part of the microwire, while the rest (unbiased) remains stress insensitive. Moving the magnet along the microwire, the stress profile can be reproduced. To realise this method in practice, some bridge circuit will be needed to compensate the microwire impedance in zero field. In this case, the voltage response caused by the change of the impedance of the activated part will be measured against zero ground level.

4. Summary and conclusions

The necessary physical conditions to study the tensile stress sensitivity of the high frequency impedance of ferromagnetic

glass-coated microwires have been established on the basis of the simple magnetostatic and impedance models. For a glass-coated Co-based microwire having a small negative magnetostriction, the high frequency impedance becomes stress-sensitive in the presence of a weak axial DC bias magnetic field. Regular and monotonous stress impedance characteristics can be obtained for excitation frequencies within 1–40 MHz. The impedance stress sensitivity (Ω/Pa) can be tuned by applying different axial DC bias magnetic fields. The highest stress sensitivity is achieved with a bias field of the order of the initial anisotropy field (corresponding to zero stress). It has been shown that the external tensile stress saturating the microwire impedance is defined by the residual axial tensile stress formed on the metal core/glass shell interface of the microwire during its fabrication. This property can be used to design microwires whose magnetic properties fit their mechanical properties. The principle of non-local stress monitoring using a long embedded microwire has been proposed. Measuring the total microwire impedance when a DC bias field is applied locally, it becomes possible to reproduce the actual stress profile along the microwire. The comparison of experimental stress impedance characteristics and their models reveals a principal discrepancy indicating that post-cure stresses accumulated in the matrix (which cannot be easily taken into account in the model) may strongly affect the sensor performance.

At the current stage of research, it would be too early to expect complete practical recommendations for the proposed method. However, the ability to measure internal micro-stresses has fairly obvious application as a laboratory test sensor. The prospect of field applications will depend on the solution of numerous technological and technical problems, including the thermal stability of impedance and the reliability of electrical contacts between the microwire and the external electronics.

Acknowledgments

We are deeply grateful to the collective of MFTI Ltd. (www.microwires.com), Republic of Moldova, and especially their director, Mr. Vladimir Larin, for providing the glass-coated ferromagnetic microwires. The authors would like to thank technician colleagues at Plymouth University: Terry Richards and Nicholas Fry, for their help in conducting the stress and impedance measurements, and Dr Richard Cullen, for his expert assistance in manufacturing the epoxy resin samples.

References

[1] Chiriac H, Ovari T-A. Amorphous glass-covered magnetic wires: preparation, properties. Appl Progr Mater Sci 1996;40:333–407.
[2] Zhukov A, Zhukova V. Magnetic properties and applications of ferromagnetic microwires with amorphous and nanocrystalline structure. New York: Nova Science Publishers; 2009.
[3] Vazquez M, Chiriac H, Zhukov A, Panina L, Uchiyama T. On the state-of-the-art in magnetic microwires and expected trends for scientific and technological studies. Phys Status Solidi A 2011;208:493–501.
[4] Qin FX, Peng H-X, Pankratov N, Phan MH, Panina LV, Ipatov M, et al. Exceptional electromagnetic interference shielding properties of ferromagnetic microwires enabled polymer composites. J Appl Phys 2010;108:044510–5.
[5] Ababei G, Chiriac H, David V, Dafinescu V, Nica I. Omni-directional selective shielding material based on amorphous glass coated microwires. Rev Sci Instrum 2012;83:014701–5.
[6] Qin FX, Peng H-X, Chen Z, Hilton G. Microwave absorption of structural polymer composites containing glass-coated amorphous microwires. IEEE Trans Magn 2013;49:4245–8.
[7] Panina L, Mohri K. Magneto-impedance effect in amorphous wires. Appl Phys Lett 1994;65:1189–91.
[8] Knobel M, Pirota KR. Giant magnetoimpedance: concepts and recent progress. J Magn Magn Mater 2002;242(245):33–40.
[9] Mohri K, Humphrey FB, Panina LV, Honkura Y, Yamasaki J, Uchiyama T, et al. Advances of amorphous wire magnetics over 27 years. Phys Status Solidi A 2009;206:601–7.
[10] Fernando GF. Fibre optic sensor systems for monitoring composite structures. Reinf Plast 2005;49:41–9.
[11] Peters K. Polymer optical fiber sensors – a review. Smart Mater Struct 2011;20:013002–18.
[12] Torrents JM, Mason TO, Garboczi EJ. Impedance spectra of fiber-reinforced cement-based composites. A modeling approach. Cem Concr Res. 2000;30:585–92.
[13] Hixson AD, Woo LY, Campo MA, Mason TO, Garboczi EJ. Intrinsic conductivity of short conductive fibers in composites by impedance spectroscopy. J Electroceram 2001;7:189–95.
[14] Peled A, Torrents JM, Mason ThO, Shah SP, Garboczi EJ. Electrical impedance spectra to monitor damage during tensile loading of cement composites. ACI Mater J 2001;98:313–22.
[15] Torrents JM, Mason TO, Peled A, Shah SP, Garboczi EJ. Analysis of the impedance spectra of short conductive fiber reinforced composites. J Mater Sci 2001;36:4003–12.
[16] Hou TC, Lynch JP. Electrical impedance tomographic methods for sensing strain fields and crack damage in cementitious structures. J Intel Mater Syst Struct 2009;20:1363–79.
[17] Kubicka M, Mahrholz T, Kühn A, Wierach P, Sinapius M. Magnetostrictive properties of epoxy resins modified with Terfenol-D particles for detection of internal stress in CFRP. Part 1: materials and process. J Mater Sci 2012;47:5752–9.
[18] Kubicka M, Mahrholz T, Kühn A, Wierach P, Sinapius M. Magnetostrictive properties of epoxy resins modified with Terfenol-D particles for detection of internal stress in CFRP. Part 2: evaluation of stress detection. J Mater Sci 2013;48:6578–84.
[19] Makhnovskiy D, Panina L. Field dependent permittivity of composite materials containing ferromagnetic wires. J Appl Phys 2003;93:4120–9.
[20] Reynet O, Adenot A-L, Deprot S, Acher O. Effect of the magnetic properties of the inclusions on the high-frequency dielectric response of diluted composites. Phys Rev B 2002;66:094412–20.
[21] Qin FX, Peng H-X. Ferromagnetic microwires enabled multifunctional composite materials Progr. Mater Sci 2013;58:183–259.
[22] Qin FX, Peng H-X, Tang J, Qin L-Ch. Ferromagnetic microwires enabled polymer composites for sensing applications. Compos A Appl Sci Manuf 2010;41:1823–8.
[23] Carbonell J, García-Miquel H, Sánchez-Dehesa J. Double negative metamaterials based on ferromagnetic microwires. Phys Rev B 2010;81:024401–6.
[24] Panina LV, Ipatov M, Zhukova V, Zhukov A, Gonzalez J. Microwave metamaterials with ferromagnetic microwires. Appl Phys A: Mater Sci Process 2011;103:653–7.
[25] Carignan L-Ph, Yelon A, Menard D, Caloz Ch. Ferromagnetic nanowire metamaterials: theory and applications. IEEE Trans Microw Theor Tech 2011;59:2568–86.
[26] Liu L, Rozanov KN, Abshinova M. Tunable properties of microwire composites at microwave frequency. Appl Phys A: Mater Sci Process 2013;110:275–9.
[27] Makhnovskiy DP, Panina LV, Garcia C, Zhukov AP, Gonzalez J. Experimental demonstration of tunable scattering spectra at microwave frequencies in composite media containing CoFeCrSiB glass-coated amorphous ferromagnetic wires and comparison with theory. Phys Rev B 2006;74:064205–15.
[28] Chiriac H, Ovari T-A. Magnetic properties of amorphous glass-covered wires. J Magn Magn Mat 2002;249:46–54.
[29] Zhukov A, Zhukova V, Blanco JM, Cobeño AF, Vazquez M, Gonzalez J. Magnetostriction in glass-coated magnetic microwires. J Magn Magn Mat 2003;258/259:151–7.
[30] Zhukov A, Zhukov V, Blanco JM, Gonzalez J. Recent research on magnetic properties of glass-coated microwires. J Magn Magn Mat 2005;294:182–92.
[31] Sablik MJ, Jiles DC. Modeling the effect of torsional stress on hysteretic magnetization. IEEE Trans Magn 1999;35:498–504.
[32] Aharoni A. Introduction to the theory of ferromagnetism. Oxford University Press; 2002.
[33] Panina LV, Sandacci SI, Makhnovskiy DP. Stress effect on magneto-impedance (MI) in amorphous wires at GHz frequencies and application to stress-tuneable microwave composite materials. J Appl Phys 2005;97:013701–6.
[34] Makhnovskiy DP, Panina LV, Mapps DJ. Field-dependent surface impedance tensor in amorphous wires with two types of magnetic anisotropy: helical and circumferential. Phys Rev B 2001;63:144424–40.
[35] Illston JM, Domone PLJ, editors. Construction materials: their nature and behaviour. Spon Press; 2010.
[36] Adenot-Engelvin A-L, Dudek Ch, Bertin F, Acher O. Thermal stability up to 400 °C of the magnetic properties of Finemet-based nanocrystallized glass-coated microwires. J Magn Magn Mat 2007;316:831–3.
[37] Sandacci SI, Makhnovskiy DP, Panina LV. Valve-like behavior of the magnetoimpedance in the GHz range. J Magn Magn Mat 2004;272/276:1855–7.